A stochastic parameterization of ice sheet surface mass balance for the Stochastic Ice-Sheet and Sea-Level System Model (StISSM v1.0)

Lizz Ultee[1,2], Alexander A. Robel[1], and Stefano Castruccio[3]

[1]School of Earth and Atmospheric Sciences, Georgia Institute of Technology, Atlanta, GA, USA
[2]Department of Earth & Climate Sciences, Middlebury College, Middlebury, VT, USA
[3]Department of Applied and Computational Mathematics and Statistics, University of Notre Dame, Notre Dame, IN, USA
Correspondence: Lizz Ultee (eultee@middlebury.edu)

Abstract. Many scientific and societal questions that draw on ice sheet modelling could be best addressed by sampling a wide range of potential climatic changes and realizations of internal climate variability. For example, coastal planning literature demonstrates a demand for probabilistic sea-level projections with quantified uncertainty. Further, robust attribution of past and future ice sheet change to specific processes or forcings requires a full understanding of the space of possible ice sheet
5   behaviors. The wide sampling required to address such questions is computationally infeasible with sophisticated numerical climate models at the resolution required to accurately force ice sheet models. Stochastic generation of climate forcing of ice sheets offers a complementary alternative. We construct a stochastic generator of Greenland Ice Sheet surface mass balance in time and space. We find that low-order autoregressive models are sufficient to accurately reproduce the interannual variability in process-model simulations of recent Greenland surface mass balance at the glacier-catchment scale. We account for spatial
10   correlations among glacier catchments using sparse covariance techniques, and we apply an elevation-dependent downscaling to recover gridded surface mass balance fields suitable for forcing an ice sheet model while including feedbacks to ice sheet surface elevation. The efficiency gained in the stochastic method supports large ensemble simulations of ice sheet change in a new stochastic ice sheet model. We provide open source Python workflows to support use of our stochastic approach for a broad range of applications.

1 Introduction

Many decision-making contexts demand probabilistic projections of sea-level rise. For example, urban planners managing coastal risks would like to be able to quantify the probability of certain levels of sea-level rise (Walsh et al., 2004) so that they can apply their own risk tolerance to assess proposed interventions (Kopp et al., 2014; Hinkel et al., 2019). Probabilistic projections can also help illustrate the benefits of climate mitigation actions for policy-makers, quantify coastal adaptation needs,
20   and identify priority areas for further research (Jevrejeva et al., 2019, and references therein). Efforts to generate probabilistic projections of future sea level change have been ongoing for decades (Titus and Narayanan, 1996), but the ice sheet component remains a source of poorly quantified uncertainty (Le Cozannet et al., 2017; Sriver et al., 2018; Jevrejeva et al., 2019).

Generating probabilistic projections of ice sheet contribution to sea level requires running many climate and/or ice sheet model simulations that can explore multiple realizations of an uncertain future. The spectrum of methods available to generate

25 future projections of ice sheet change makes that task difficult. The most computationally efficient methods find an empirical relationship between some climate variable, often global mean surface temperature, and a variable of interest, such as global mean sea level (Rahmstorf, 2007) or ice sheet melt (Luo and Lin, 2022). Such methods allow wide sampling of future climate scenarios, which is necessary to account for scenario uncertainty. However, they assume that the form of the relationship between the variables will remain the same in the future, which is not assured in a rapidly changing climate with feedbacks

30 among multiple variables. The structural uncertainty in those methods—that is, the uncertainty attributable to poor knowledge of the form of the model itself—is therefore high, and their results are difficult to convert into a probability distribution.

More sophisticated numerical models represent physical processes, such as ice sheet flow, snowfall, and surface melting directly (Goelzer et al., 2020; Seroussi et al., 2020), explicitly modeling changes over time in the relationship between climate forcing and output variables of interest. Such models include many more parameters and internal variability of processes on a

35 wide range of spatial and temporal scales. A direct representation of physical processes helps to constrain structural uncertainty related to processes and internal variability, but the computational expense of sophisticated models limits the number of future scenarios that can be sampled. Model outputs thus represent discrete points in a wide range of possibilities, providing too little information to estimate the probability distribution of output variables such as future sea level.

A particular obstacle to large ensemble simulations of future ice sheet evolution is the computational expense of generating

40 surface mass balance forcing. "Surface mass balance" ("SMB") refers to the set of processes through which ice sheets gain and lose mass at the ice sheet interface with the atmosphere. Mass-gain processes include precipitation, vapor deposition, and refreezing of meltwater; mass-loss processes include melting (with subsequent runoff) and sublimation. Due to the complex set of ice-atmosphere interactions that comprise mass balance, ice sheet models are not typically forced directly by climate model output. Rather, climate model output must be used to construct an SMB field, often through use of a specialized mass balance

45 model that accounts for on-ice processes (see e.g. Fettweis et al., 2020, and references therein). Increasing sophistication in the process-based models used to construct ice sheet SMB means a corresponding increase in computational demand for each individual simulation with these models.

Stochastic methods provide a low-cost alternative to sophisticated process models (Sacks et al., 1989). Previous studies have applied stochastic methods to analyze ice sheet mass balance observations with the primary aim of testing whether a trend

50 emerges from the range of natural variability. For example, Wouters et al. (2013) represented SMB simulated by RACMO2 as an order-p autoregressive process to estimate the uncertainty on mass balance trends for the Greenland and Antarctic Ice Sheets. More recent studies tested multiple types of stochastic models to characterize the variability in Antarctic SMB (Williams et al., 2014; King and Watson, 2020) and thereby test the presence of significant, detectable trends in SMB observations. Here, we have a different aim: to construct a statistical generator of SMB to force an ice sheet model, which should include interannual

55 variability at the catchment scale, temporal trends, seasonality, and spatial variation down to the scale of an ice sheet model mesh. We approximate the output of a process-based SMB model as one realization of a stochastic process. The statistical model that produces a realization best fit to the process-based model output can then be used to generate hundreds of other realizations, representing a range of possibilities for future SMB, at much reduced computational expense. Those possibilities support large ensemble simulations of ice sheet change, including simplified feedback of ice sheet geometry on SMB. To best

60 support the broader glaciological community, we base our method entirely on open-source software packages and provide our own open-source code where necessary.

Below, we present the data sources that informed our construction of a stochastic mass balance generator (§2). We then describe our choice of temporal model type and how we selected the best-fit model for each catchment of the Greenland Ice Sheet (§3.1 - 3.2) . Section 3.3 describes how we accounted for large-scale covariance in SMB across the ice sheet. We

65 demonstrate the generation of forward-projected SMB time series (§3.4) and how to downscale those time series to ice sheet model grid scale (§3.5). Finally, we contextualise our work with previous studies and highlight its potential applications (§4).

2 Data

First, we will examine ice core reconstructions of SMB in Greenland over the last 2000 years (Andersen et al., 2006). The point nature of these measurements makes them unsuitable for generating stochastic, ice-sheet-wide SMB fields, but they are

70 a useful benchmark to assess the characteristic time scales of SMB variability, including time scales longer than are simulated in regional SMB models.

We next will proceed to construct the stochastic SMB model based on SMB fields output from high-resolution regional climate models with domains encompassing the Greenland Ice Sheet. Here, we focus on output from 7 models that participated in the Greenland SMB Model Intercomparison Project ('GrSMBMIP'; Fettweis et al., 2020) to determine whether stochastic

75 generator type/order is dependent on the choice of process model. These benchmark SMB models have been extensively validated against observations over recent decades. The GrSMBMIP regional models are all forced at their boundaries by ERA-Interim reanalysis data and have been processed onto a common 1km square grid, with a common ice extent mask applied.

We aggregate each SMB model output field for each outlet glacier catchment at an annual time scale. We overlay each field

80 with the catchment outlines (Figure 1) provided by Mouginot and Rignot (2019) and use Delaunay triangulation to produce a covering of each catchment area. We average SMB over the grid point closest to (or within) each triangle of a catchment to arrive at catchment mean SMB for each month, catchment and model from 1980 to 2012. We then average over annual time scales so that the subsequent analysis produces statistical models of inter-annual variability. SMB variability at the inter-monthly time scale is dominated by the seasonal cycle, which is added back to generated SMB time series through downscaling

85 (Section 3.5).

3 Model description

3.1 Temporal model for catchment-averaged annual SMB

We fit a generative statistical model for catchment-averaged SMB using an approach adapted from the work of Hu and Castruccio (2021) on other climate fields. We define the n dimensional vector $\mathbf{M}(t)$ to be the catchment-averaged SMB in each of
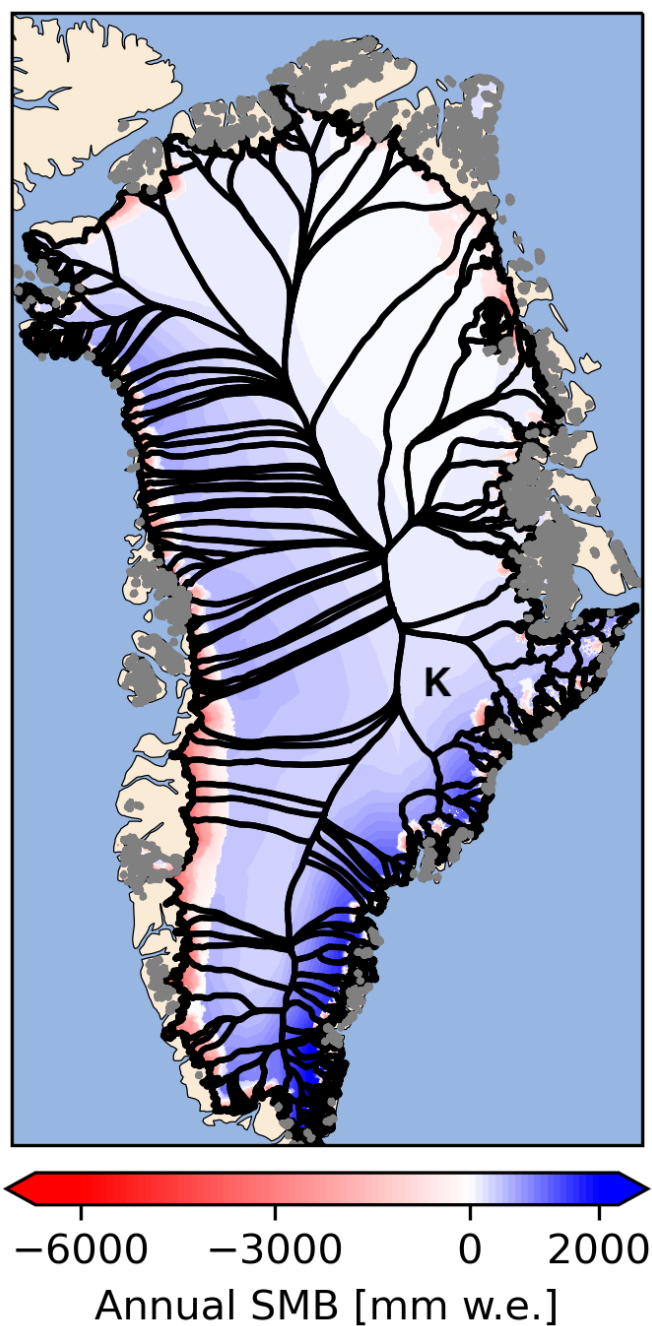
Figure 1. Catchments from Mouginot and Rignot (2019) used to aggregate ice-sheet-wide mass balance. Grey outlines indicate catchments that are not simply connected, for example several small glaciers that do not intersect but were grouped together for the Mouginot analysis. Color contour shading illustrates annual mass balance for an example year (2010), taken from the dEBM contribution to SMBMIP (Fettweis et al., 2020; Krebs-Kanzow et al., 2021). The 'K' marker indicates the Kangerlussuaq Glacier catchment, for which example time series and fitting procedure are shown in the following figures.

n catchments at time t, and we assume that it can be described by an additive model with a temporal variability vector $\boldsymbol{\mu}(t)$ and an error term vector $\boldsymbol{\epsilon}(t)$ of the form:

$$\mathbf{M}(t) = \boldsymbol{\mu}(t) + \boldsymbol{\epsilon}(t), \tag{1a}$$

$$\boldsymbol{\mu}(t) = \boldsymbol{\beta}_0 + \boldsymbol{\beta}_1 f(t) + \sum_{i=1}^{p} \boldsymbol{\Phi}_i \cdot \mathbf{M}(t-i), \tag{1b}$$

$$\boldsymbol{\epsilon}(t) \sim \mathcal{N}(0, \boldsymbol{\Sigma}). \tag{1c}$$

In the example case we present here, the vectors $\mathbf{M}, \boldsymbol{\mu}, \boldsymbol{\varepsilon}$ have one entry for each of the $n = 200$ catchments at time t, and we evaluate each at a total of $m = 30$ time steps.

The temporal trend $\boldsymbol{\mu}(t)$ includes historical mean SMB for each catchment $\boldsymbol{\beta}_0$, and a linear relationship with $f(t)$, the forcing variable, $\boldsymbol{\beta}_1(t)$. The forcing variable, $f(t)$, can be an external process which causes slow changes in SMB, such as atmospheric temperature ($f(t) = T_A(t)$) or simply a prescribed dependence on time (e.g., $f(t) = t$). Finally, Equation 1b includes autoregressive terms up to order p contained in the diagonal matrices $\boldsymbol{\Phi}_i, i = 1, \ldots, p$. The temporal trend as written would thus approximate an autoregressive process of order p, AR(p). Section 3.2 discusses how we identified AR(p) as the best type of temporal model for this application. At this stage, fitting temporal models to annually-aggregated time series, we exclude seasonal terms from the temporal trend $\boldsymbol{\mu}(t)$; seasonality is incorporated deterministically during the downscaling process described in Section 3.5. All stochasticity in this generation technique enters through inter-annual variability.

The error term $\boldsymbol{\epsilon}(t)$ is assumed to be independent, identically distributed in time and from an n dimensional normal distribution with mean of zero and covariance matrix $\boldsymbol{\Sigma}$. As we describe in Section 3.3, spatial correlations between catchments are captured in $\boldsymbol{\epsilon}(t)$.

3.2 Selecting candidate model type and order

We tested several model types in search of the most appropriate way to represent interannual SMB variability in Equation 1b. Three criteria inform our selection of candidate stochastic model types for temporal SMB variability. First, we would like our candidate temporal models to capture the time scales of variability apparent in the data, based on standard statistical methods that are likely to be familiar to glaciologists. Second, we would like our methods to build on existing open-source software, such that other researchers can test and apply our work. For that reason, we prioritize models with existing fitting routines in Python or R. Finally, we would like to be able to compare our findings to those of King and Watson (2020) for the Antarctic Ice Sheet, so we prioritize temporal model families that those authors also tested.

These criteria guide our investigation of three common types of autoregressive-fractionally integrated moving average (ARFIMA) models. AR(p) models are the simplest of the ARFIMA family. They assume that the value of SMB at time t depends linearly on values of SMB at times $(t-1, t-2, ..., t-p)$. The second type, ARIMA models of order (p, d, q), include order-p autoregressive terms applied to a series that has been differenced d times to reach stationarity, as well as dependence on a weighted moving average of the past q residual error terms. General ARFIMA models are similar to ARIMA models but

allow non-integer values for d, accounting for 'long memory' in the time series. King and Watson (2020) tested AR(p) and ARIMA models; they also tested Generalized Gauss-Markov models, for which we were unable to find an open-source fitting routine, but which are very similar to ARFIMA models of order $(p, d, 0)$.

For each catchment, we estimate $\boldsymbol{\beta}_0$ as the 1980-2012 mean and remove it from the series. We then use Conditional Maxi-
125 mum Likelihood (Ordinary Least Squares) to optimize values of $\boldsymbol{\beta}_1$ and the remaining parameters of Equation 1b associated with each candidate model type (AR, ARIMA, ARFIMA) over a range of orders (p, d, q). We perform the model fitting with built-in functions from the Python package statsmodels v0.12.2 (Seabold and Perktold, 2010): `statsmodels.tsa.ar_model.AutoReg` and `statsmodels.tsa.arima.model.ARIMA`. Statsmodels does not include a built-in function to fit ARFIMA models, so we apply fractional differencing following Kuttruf (2019) and subsequently test ARIMA$(p, 0, q)$ with the built-in function. For a
130 given model, statsmodels reports metrics of fit including the Akaike Information Criterion (AIC) and Bayesian Information Criterion (BIC). We choose to select for minimum BIC to encourage simpler model choice (as in King and Watson, 2020). We compare the BIC of the best-fit models for each catchment series to identify the most suitable class of models.

To decide the range of orders (p, d, q) to test in our model fitting, we use the autocorrelation and partial autocorrelation functions ("ACF" and "PACF" respectively) to target the relevant time scales of variability. In a purely autoregressive process,
135 the number of values significantly different from 0 before the first non-significant value in the PACF would indicate the AR order p. In a purely moving-average process, the number of values significantly different from 0 before the first non-significant value in the ACF would indicate the MA order q. These metrics cannot be used to determine the order (p, d, q) of a more general ARFIMA process, but we use them as qualitative indicators of an appropriate range for testing. Ice core-derived ACF and PACF show significant values at time scales of up to five years, tapering to values not significantly different from 0 at
140 longer time scales (Figure 2). In each ice core, there are some significant autocorrelations at lags >10 years, but which long lags have significant PACF differs by core. All cores agree on several lags ≤5 years with significant PACF. We therefore choose to test values of p and q from 1 to 5. We determine the order of differencing required to reach stationarity, d, using Augmented Dickey-Fuller and KPSS tests of stationarity on each catchment time series. Both tests agreed that the de-meaned catchment average time series were stationary, so $d = 0$ should be appropriate, but for completeness we also tested $d = 0.5$ and $d = 1$.
145 Among the range of values (p, d, q) tested, we select the best fit model as the one with the lowest BIC.

In every catchment and SMB model tested (1400 catchment-model pair time series tested), AR models were the most suitable. Figure 3b shows example best fits for four model types and their BIC (see legend). We can interpret BIC differences larger than 100 with a very strong preference for AR(n) models over ARIMA and ARFIMA models. Further, low-order AR models are a universally acceptable fit to catchment-aggregated SMB in Greenland. AR(1) models were preferred in 174 out
150 of 200 catchments. In catchments with best-fit models of a higher order, the difference in BIC between the best-fit model and an AR(1) model was always less than 1. Such a small difference indicates a very weak preference for one model type over another. That is, the fit of a higher-order autoregressive model to the process-model series is statistically indistinct from the fit of an AR(1) model. We conclude that AR(1) models offer an acceptable fit to catchment-averaged SMB for all 200 catchments we tested, which captures the dominant mode of interannual SMB variability with a low-order model. The AR(1) fit shown
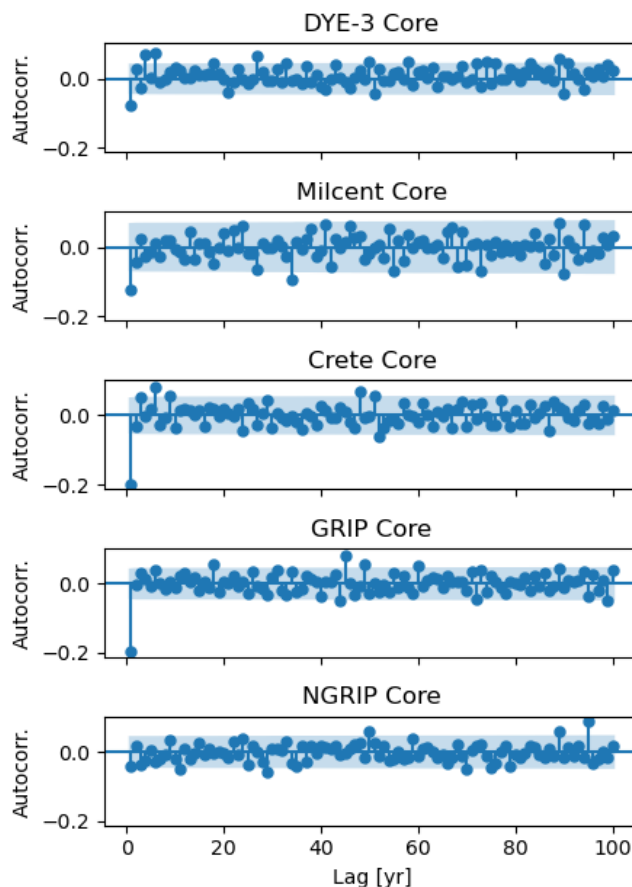
Figure 2. Example autocorrelation function of SMB derived from five Greenland ice cores, with time horizon out to 100 years. Shaded area shows the 95% confidence interval around 0, such that points outside the shaded area indicate autocorrelations that are significantly different from 0.

155   in Figure 3b has relatively low amplitude interannual variability; the residual variability may be captured in the spatial noise generation (§3.3) or the downscaling (§3.5), or the user may decide that the higher-order AR(4) fit is more appropriate.

3.3   Estimating SMB covariance between catchments

Thus far, we have described a method for fitting and generating time-varying SMB for individual catchments with no correlation beyond the catchment scale. However, SMB over the Greenland Ice Sheet may vary coherently at spatial scales beyond those

160   of single outlet glacier catchments due to large-scale processes in atmospheric circulation (Lenaerts et al., 2019). Motivated by this physical intuition, we introduce spatially-informed noise generation.
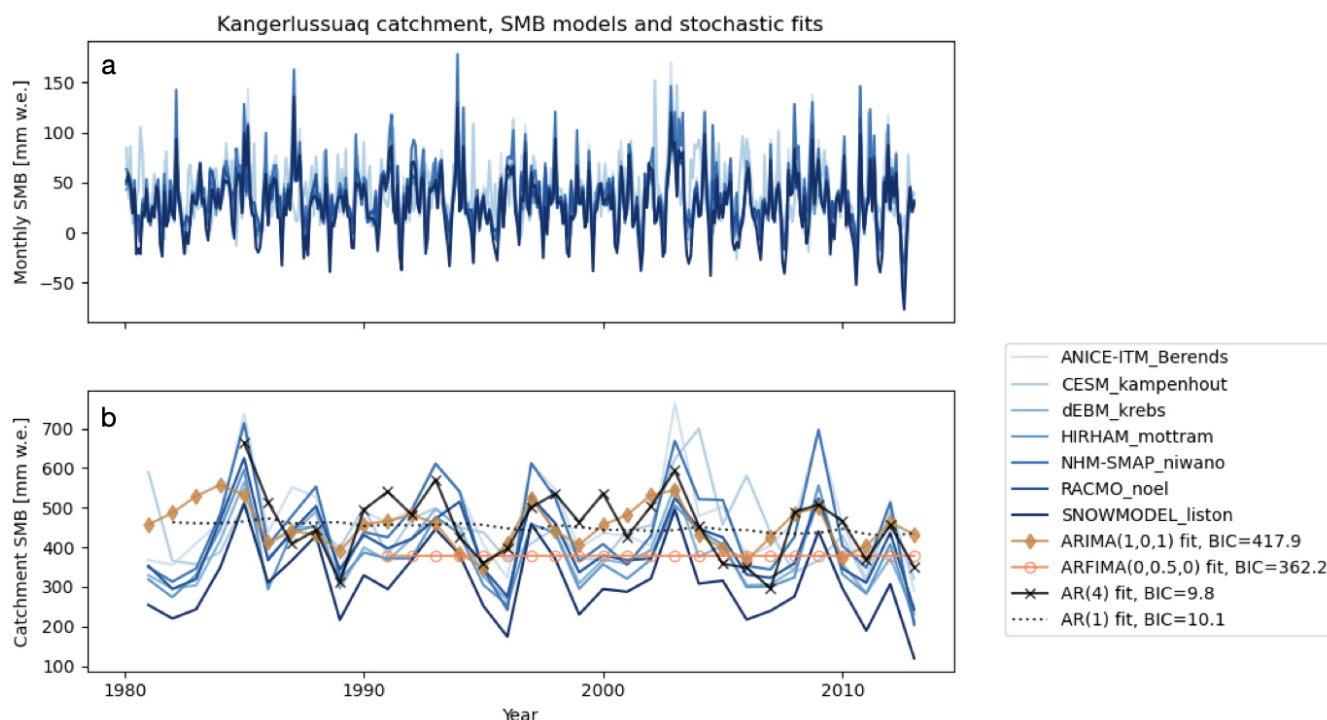
Figure 3. Catchment-mean SMB from seven Greenland-wide models. Panel (a): time series at monthly scale, as originally presented in the model output data. Panel (b): time series summed to annual scale, with series from example best-fit stochastic generators overlaid. The Bayesian Information Criterion for each model's fit to an example process model (NHM-SMAP) is shown in the figure legend. Lower BIC values indicate more preferred models.

Following Hu and Castruccio (2021), we construct a matrix of variance Σ for catchment-level error terms (Equation 1c above) as:

$$\Sigma = \mathbf{DCD}, \tag{2}$$

165 where $\mathbf{D}$ is the diagonal matrix of per-catchment standard deviations and $\mathbf{C}$ is the spatial correlation matrix among all catchments. We calculate the empirical correlation matrix $\hat{\mathbf{C}}$, which is an approximation of $\mathbf{C}$, from the residuals of per-catchment best-fit models described in Section 3.2. We save each residual (length $n = 30$) to an array of length $m = 200$, one entry for each catchment. The empirical correlation matrix $\hat{\mathbf{C}}$ is then the matrix of correlation coefficients of the residuals, which we compute using `numpy.corrcoef()` as below:

```
1  ar_resids = []
2  for i in range(1,200):
3      s = read_catchment_series(filepath, anomaly=True)
4      mod = AutoReg(series, n=1, trend='ct', seasonal=False).fit()
```

```
5      r = mod.resid
6      ar_resids.append(r)
7  ar_resids -= np.mean(ar_resids, axis=0)
8  empirical_C = np.corrcoef(ar_resids)
```

Because the number of catchments we seek to simulate ($m = 200$ for Greenland) is considerably larger than the number of data points used to train individual statistical models (30 years of catchment-aggregated SMB for each catchment), $\hat{\mathbf{C}}$ is singular. Therefore, we must enforce a sparsity condition to reduce the influence of spurious information. We estimate a sparse correlation matrix $\mathbf{\Gamma}$ using the graphical lasso algorithm described in Friedman et al. (2007).

We apply the `GraphicalLassoCV` function from the Python package *scikit-learn* v0.24.2 (Pedregosa et al., 2011), which estimates a sparse correlation matrix $\mathbf{\Gamma}$ with the following formulation:

$$\mathbf{\Gamma} = \mathrm{argmin}_K \left(\mathrm{tr}\, \hat{\mathbf{C}}\mathbf{K} - \log \det \mathbf{K} + \alpha \|\mathbf{K}\|_1 \right), \tag{3}$$

where $\mathbf{K}$ is the inverse correlation matrix and α is a positive regularization parameter. Higher values of α lead to sparser resulting matrices $\mathbf{\Gamma}$.

3.4 Forward modelling

Finally, we generate a set of realizations of the forward stochastic generator. Each realization is the sum of an autoregressive component and a draw $\epsilon(t)$ from the normal distribution with spatial covariance, as described in Equation 1a and Section 3.3. We find the Cholesky decomposition $\mathbf{\Gamma} = \mathbf{L}\mathbf{L}^{\mathbf{T}}$ of the sparse correlation matrix, and use the lower-triangular component to generate spatially informed noise. The draw $\epsilon_k(t)$ for the kth catchment is found by matrix multiplication:

$$\epsilon_k(t) = \mathbf{D}\mathbf{L}\,\mathbf{N_j}\,\hat{k} \tag{4}$$

where $\mathbf{N_j}$ is a random normal matrix of shape (m, Y) for m the number of catchments, Y the number of years in the desired time series, and $\hat{k}$ selects the kth row of the matrix.

We generate realizations of catchment-mean SMB for an example catchment, Kangerlussuaq Glacier. Each realization is a single time series of catchment-mean SMB with variability described by the stochastic generator. Figure 4 shows 10 realizations of Kangerlussuaq SMB from 1980-2050, with process model training data overlaid in black for 1980-2012. By inspection, the stochastic realizations (blue lines on Figure 4) have variability of similar amplitude and time scale to the process model series. The 10 realizations, generated in a few seconds on a laptop, fill the expected range of uncertainty in annual SMB. We interpret that these stochastic realizations are an efficiently generated forcing for ensemble simulations of ice sheet change given uncertain SMB.

A user generating realizations of SMB at a particular location, or aggregated over some area, could use the method described up to this point. For example, this method could generate realizations of aggregated SMB to support detection of departures from background variability, as in Wouters et al. (2013). The next section describes how to downscale SMB from the catchment annual-average to spatially extensive SMB fields at sub-annual time scales.
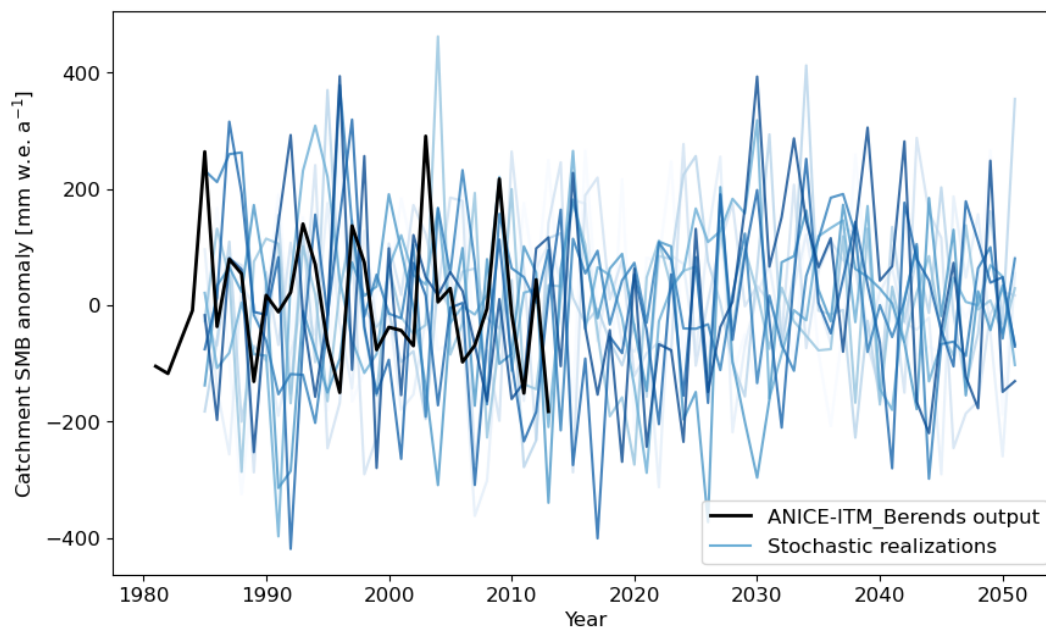
Figure 4. Forward simulation of Kangerlussuaq catchment SMB to 2050, with 1980-2010 mean removed, generated using an AR(4) model with spatially-informed noise. The black line shows the results of the process model ANICE-ITM during the period simulated for GrSMB-MIP. Blue lines are single realizations of the stochastic generator.

3.5 Elevation downscaling

To force an ice sheet model, we require a two-dimensional SMB field on the mesh of the model, rather than catchment-aggregated time series. We now apply a spatial and temporal downscaling approach to produce gridded SMB from the stochastically generated series at sub-annual time steps. The downscaling assumes that within each glacier catchment and for a given time of the seasonal cycle, the SMB variation within a catchment can be described by a piecewise linear function with respect to elevation. This downscaling recognizes that, particularly in Greenland, there is a strong seasonal cycle in SMB and that the spatial variations of SMB within a glacier catchment are mostly a function of elevation. As shown in Figure 5, these assumptions are generally quite good for Greenland SMB, and they are reflected in other statistical downscaling approaches that have been previously applied in deterministic frameworks (Hanna et al., 2011; Wilton et al., 2017; Sellevold et al., 2019). Further, the method generates fields with realistic spatiotemporal variability and elevation dependence, which can be embedded within an ice sheet model (e.g. Verjans et al., 2022) to capture the known feedback between ice sheet surface elevation change and SMB change (Edwards et al., 2014; Lenaerts et al., 2019).

For each point $\mathbf{p}$ in a given catchment, we need the surface elevation $z(\mathbf{p})$ used to force the physical SMB model underlying our stochastic generator, and the local SMB anomaly

$$\Lambda(\mathbf{p},t) = A(\mathbf{p},t) - \overline{A}(t), \tag{5}$$

where $A(\mathbf{p}, t)$ is the process-model SMB at point $\mathbf{p}$ and time t and $\overline{A}(t)$ is the catchment mean SMB computed from the same process model at time t. We group all local elevation-anomaly pairs by month—for example, all January values together, all

215 June values together—and fit a piecewise linear mass balance gradient for each month τ:

$$
\Lambda_\tau(\mathbf{p}) = \begin{cases} c_0 + c_1 z(\mathbf{p}) & 0 < z(\mathbf{p}) \leq z_1 \\ c_0 + c_1 z_1 + c_2 z(\mathbf{p}) & z_1 < z(\mathbf{p}) \leq z_2 \\ c_0 + c_1 z_1 + c_2 z_2 + c_3 z(\mathbf{p}) & z_2 < z(\mathbf{p}) \leq z_3, \end{cases} \tag{6}
$$

where c_0 is the minimum SMB and the segment slopes (c_1, c_2, c_3) and break points (z_1, z_2) are free parameters optimized by BIC and AIC. In each catchment we thus have twelve functions Λ_τ, one for each month, which re-introduces seasonal variation. Example fits for the Kangerlussuaq Glacier catchment are shown in Figure 5.

220 Finally, we produce time series of monthly local mass balance a for each grid point $\mathbf{p}$ of the kth catchment:

$$
a(\mathbf{p}, t) = \mathbf{M}(t) \cdot \hat{k} + \Lambda_\tau(\mathbf{p}), \tag{7}
$$

where t is the time in months since the start of the series, $\mathbf{M}(t)$ is the annual catchment-mean SMB generated by the stochastic generator, and Λ_τ is the local SMB anomaly for month τ as defined above. The same principle could be adapted for training data provided at even finer temporal resolution (i.e., weekly or daily).

225 To illustrate the method, we applied the elevation-based downscaling to estimate local SMB series at two different points, distributed across elevation, in the Kangerlussuaq Glacier catchment. Figure 6b shows those time series. Blue lines are the stochastically generated SMB, downscaled to a single point in space; black lines are the process model output at the grid cell nearest to the selected point. The point represented in the bottom panel is near the terminus and shows large-amplitude seasonal and inter-annual variations in both the process model and the downscaled stochastic realizations. The stochastic realizations

230 track closely with the process model series, while also including inter-annual variability in winter and summer SMB that differs between realizations. The point in the top panel is in the accumulation area. For that point, the range among the stochastic realizations is wider than the apparent variability in the process model series. The seasonal cycle has approximately correct amplitude. We interpret that the variability in the catchment-averaged SMB is dominated by large-amplitude variation near the terminus, which is then reflected in the stochastic generator fit to the process model series. We further discuss this overestimate

235 of accumulation zone inter-annual variability in the next section.

4 Discussion

Simulating ice sheet evolution in a numerical model generally requires a two-dimensional SMB field that may vary in time. Here, we have laid the foundation for efficiently generating many realizations of a time-varying SMB field with stochastic methods. Figure 6 demonstrates that our method can produce realistic SMB time series across an outlet glacier catchment. To

240 produce a two-dimensional field, a user would apply the downscaling method described in Section 3.5 to every grid point in the catchment. The piecewise linear mass balance gradients shown in Figure 5 (insets) are provided to the user as mathematical
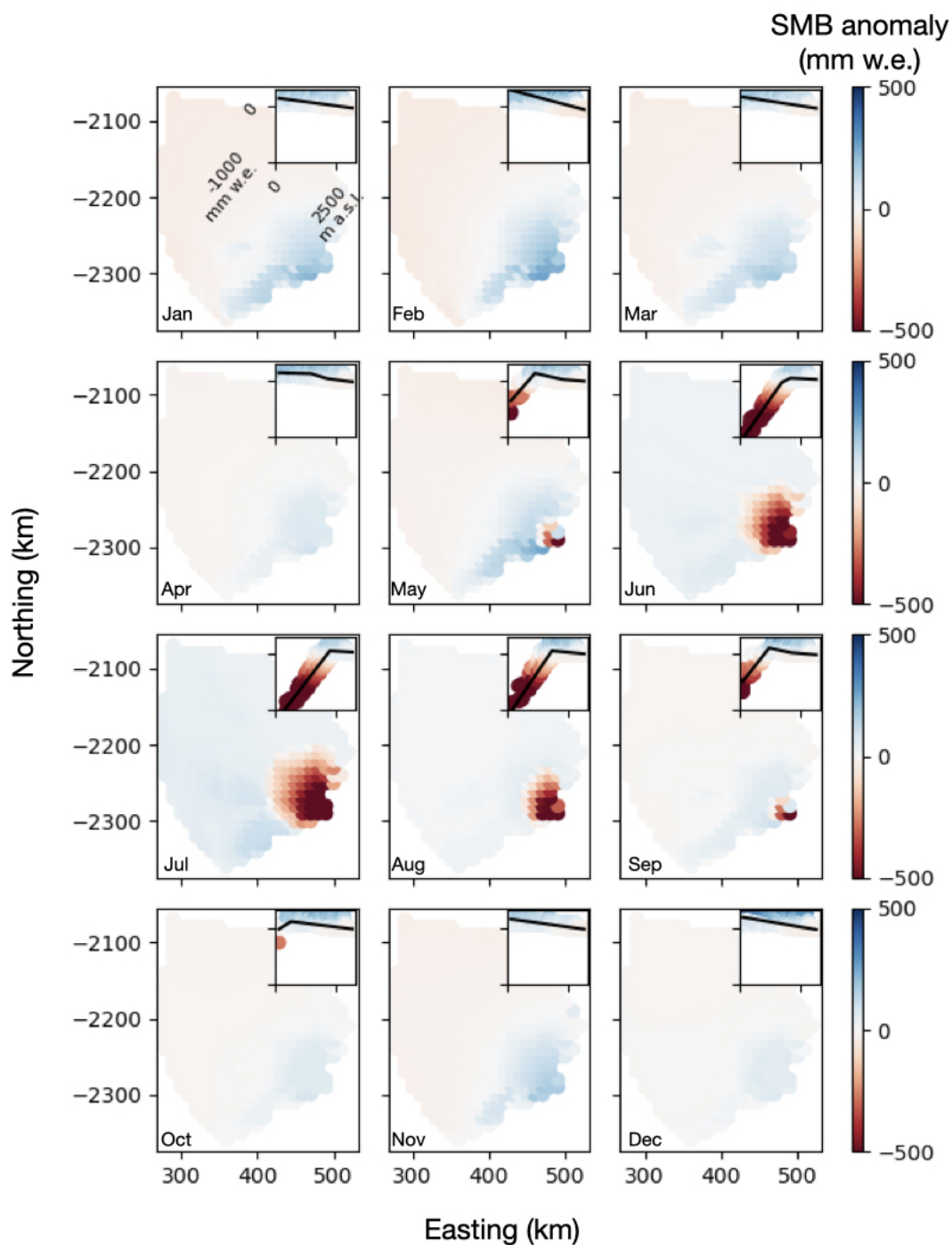
Figure 5. Monthly SMB anomaly (difference from catchment mean) for each point within the Kangerlussuaq Glacier catchment, based on the ANICE-ITM model contribution to GrSMBMIP; and (insets) SMB lapse rate with elevation for each month, deduced from the anomaly fields shown. Colormaps are consistent for all panels.
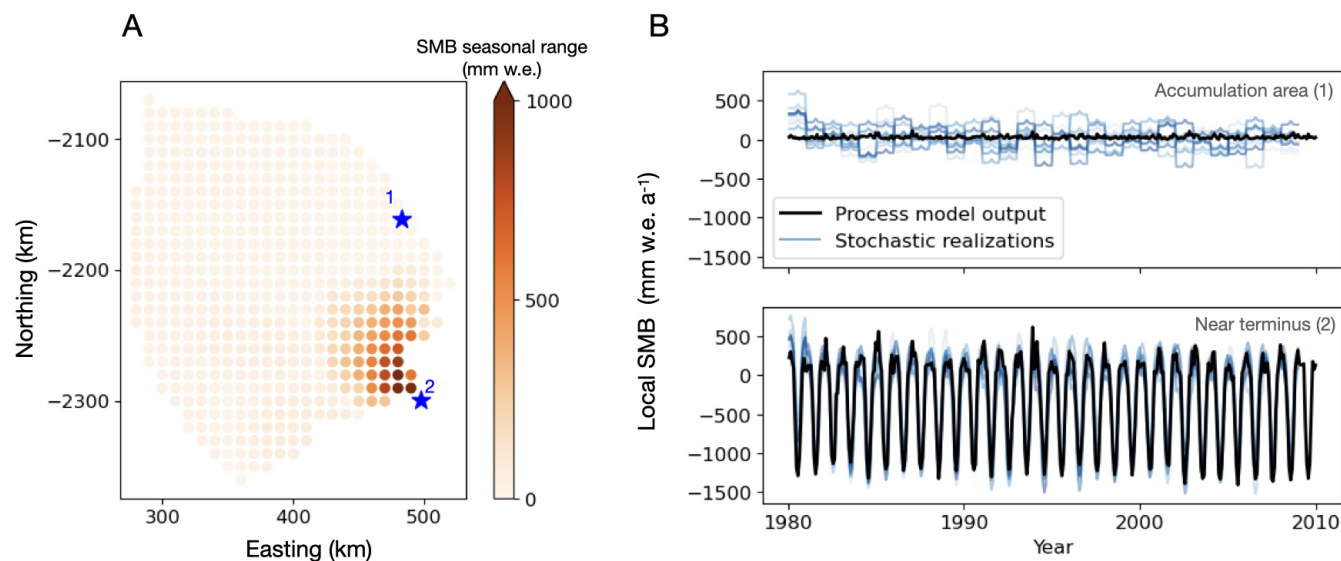
Figure 6. (A) Location of example points (blue stars and numbers) in the Kangerlussuaq Glacier catchment. Circle markers show SMBMIP grid points, colored by the seasonal range in mass balance at that location, computed as local mass balance in December minus local mass balance in July. (B) SMB time series scaled from catchment mean down to local (single grid point) values. The upper series are scaled to Point 1, in the accumulation area; the lower series are scaled to Point 2, near the terminus. As in previous plots, the black lines in each series are process model output and the blue lines are stochastic realizations. Series share x and y axes.

functions, so the downscaling can be applied on whatever mesh the user provides. This simplicity also allows this method to be incorporated directly into an ice sheet model so that feedback of changing ice sheet geometry on SMB is included, in addition to the SMB variability in space and time generated by the method described above. This stochastic SMB generation method

245 has been incorporated directly into the Ice Sheet and Sea-level System Model (Verjans et al., 2022).

In evaluating candidate stochastic generators for catchment annual mean SMB, we found the best fit to process-model variability with the lowest order statistical models. For all 200 catchments we tested, simple autoregressive models had by far the lowest Bayesian Information Criterion (better fit to process-model SMB) among model types (e.g. Figure 3b). Moreover, among low-order autoregressive models, first-order AR(1) models are almost universally preferred over higher-order models (or

250 not meaningfully different from higher-order models in terms of BIC). AR(1) models could have a low BIC despite relatively greater error than higher-order models, as seen in Figure 3, because the BIC penalizes excess parameters. We interpret that higher-order AR(n) models may offer the best fit to the process-model data in some catchments, but that AR(1) models are an acceptable simplification, especially in combination with the generation of spatially-informed noise based on the residuals. Regardless, users of this model selection workflow may ultimately prioritize having less error in which case higher-order AR(n)

255 models can be selected as well.

Our findings contrast with the results of a study by King and Watson (2020), which found that simple white noise and AR(1) models were not effective in capturing observed Antarctic SMB variability. For annual SMB time series, reconstructed

for 1800-2010, for four Antarctic catchments–the West Antarctic Ice Sheet, East Antarctic Ice Sheet, Antarctic Peninsula Ice Sheet, and Antarctica as a whole– King and Watson (2020) used the software Hector (Bos et al., 2013a) to simultaneously fit a linear trend and noise model. They found that white noise and AR(1) models tend to underestimate low-frequency variability, and that a better fit to observations came from power law or Generalized Gauss-Markov models (Bos et al., 2013b). The use of only 3 sub-catchments for Antarctica results in much broader spatial aggregation as contrasted with our use of 200 sub-catchments for the smaller Greenland Ice Sheet. That broad spatial aggregation might be expected to smooth short-term variability and amplify the relative importance of low-frequency variability that correlates with large-scale climate forcing. For that reason, it is not surprising that we find a better fit with simple temporal models given that we aggregate over smaller ice-sheet catchments and study a shorter time period. Further, the spectra of variability could well be different between Antarctica and Greenland; the former is a polar continent with climate heavily influenced by the Antarctic Circumpolar Current, while the latter is a large subpolar island exposed to warm oceanic currents and westerly atmospheric flow. Finally, we have tested stochastic model fit to more data sources — seven SMB process models — than did earlier studies of one or two data sources (including King and Watson, 2020); we found that simple autoregressive models were the best fit for all seven of the training models, lending credence to our results despite their contrast with earlier findings.

We chose to limit the range of lags we tested in our autoregressive model fitting for two reasons. First, the autocorrelation functions of annual SMB reconstructed from ice cores (Figure 2) show that most cores have significant autocorrelation at short lags (< 10 yr) and no consistently significant autocorrelation at longer lags. Second, higher-order autoregressive models risk both overfitting the data and needlessly adding computational expense, since high order autoregressive models require holding the SMB from many previous time steps in local memory. The Bayesian Information Criterion of a few candidate high-order AR(n) model fits to SMB data is high, supporting our choice in this case. Further, the decadal timescale on which we focus is the most feasible timescale on which to generate probabilistic projections of sea level change. For timescales of 50 years and longer, uncertainty about anthropogenic emissions scenarios dominates the range of possible sea level change (Hinkel et al., 2019). However, it should be noted that a low-order autoregressive model such as ours is poorly suited to capture low-frequency variability, which may become important for multi-century simulations.

Our ice core data analysis (Figure 2) does not suggest that we have missed major modes of variability in our model fitting, but it is still plausible that our stochastic generator fitted to 32 years of training data will fall short in reproducing multidecadal and longer variations. To ensure that our stochastic SMB does not miss low-frequency variability that could substantially change Greenland outlet glacier catchments in the coming century, and to support stochastic generation for longer-term historical simulations, further analysis should incorporate longer-term process model output or spatially resolved reconstructions of SMB from ice cores or other observations. Recent analyses also suggest that parts of the Greenland Ice Sheet may be approaching a destabilization, which could change the variance and autocorrelation timescale of its future mass balance (Boers and Rypdal, 2021). Stochastic generator fitting intended for multi-century future projection should thus be trained on output data from SMB models run at similarly long time scales, where possible including the relevant feedbacks and instabilities, rather than projecting forward from 30-year historical simulations as we have done here. We emphasize that our study describes a flexible

methodological framework for training a stochastic generator of SMB variability, and that this framework can be applied to new SMB process model outputs as they become available.

Our downscaling method makes it possible to generate SMB fields on whatever mesh is needed by a numerical ice sheet model. In ice sheet models designed to accept stochastic forcing, the parameters of the stochastic generator can be provided directly for online generation of the forcing fields within the model itself, with negligible addition of computational expense (demonstrated in Verjans et al., 2022). With regular updates to the surface elevation of each point on the model mesh, the downscaling method can also account for the known feedback between ice sheet surface elevation and surface melt rate (Hanna et al., 2013; Edwards et al., 2014; Lenaerts et al., 2019). Such a streamlined workflow will further facilitate large ensemble simulations. The downscaled time series we presented in Figure 3, which we generated with data aggregated to a standard set of catchments (Mouginot and Rignot, 2019), show variability dominated by large-amplitude seasonal variation at the terminus. This asymmetry in variability amplitude between the accumulation and ablation zones ultimately leads to some overestimation of interannual variability at accumulation zone points. We suggest that this effect could be tempered by splitting catchment data into accumulation-area and ablation-area bins before fitting the spatial downscaling function. For the purposes of forcing an ice sheet model, such disaggregation may not even be necessary, as sub-decadal outlet glacier flow variability is driven by near-terminus SMB variability (Christian et al., 2020).

The spatial covariance method we apply here will lose some relevant spatial details from the original process models. As described in Section 3.3, our empirical inter-basin correlation matrix C was singular, and in order to generate new realizations of variability, we enforced sparsity in the correlation matrix Γ. By construction, this method loses some spatial detail present in the original dataset. Further, our method does not quantify uncertainty in the model fit — for example, within-catchment differences in the best-fit statistical model parameters — other than the range of variability present in the original process-model simulations. Our stochastic generation of SMB fields based only on SMB models also disregards any covariance between oceanic and atmospheric forcings. More sophisticated methods currently under development, such as fitting a Gaussian process emulator (Mohammadi et al., 2019; Edwards et al., 2021), may be able to resolve these problems in the future. However, at present, there is too little data available from high-fidelity models of SMB to pursue spatial methods beyond what we have shown here.

Given the simplifications described above, and the abstraction of stochastic parameters as contrasted with physical quantities, we do not intend stochastic SMB generation to completely replace process-model simulation of ice sheet SMB. Rather, we envision stochastic SMB generation to provide a complementary tool set which reproduces many features of SMB process models at nearly negligible computational expense. The open source software that we have developed, and the existing packages on which it is built, can be easily applied to fit a stochastic representation to new outputs from process-based SMB models as they become available. Selecting an appropriate class of stochastic generator is the most time-consuming step of the process; with that complete, the best-fit model parameters can be updated at any time to account for new process model results, and generate hundreds of new realizations. Stochastic generation therefore serves to more immediately connect dynamic ice sheet projections with cutting-edge SMB simulations without the need for costly coupled simulations.

5 Conclusions

We have described the development and demonstrated the use of a stochastic method to generate many realizations of ice sheet SMB fields varying in space and time. For all 200 catchments of the Greenland Ice Sheet that we tested, the simplest temporal models (AR(p) with order $p < 5$) provided the best fit to process-model-derived SMB time series. Our method streamlines the creation of climate-dependent forcing to simulate ice sheet mass change at multi-decadal scale. The improved computational efficiency offered by this stochastic SMB generation method should facilitate large ensemble simulations of ice sheet contribution to sea level change, which will support probabilistic sea-level projections with improved uncertainty quantification.

Code and data availability. Code supporting our analysis is available on GitHub (https://github.com/ehultee/stoch-SMB) and [***will be archived on Zenodo pending final version of manuscript***]. Catchment-aggregated SMB time series derived from the participating models are included in a subfolder of our GitHub repository, github.com/ehultee/stoch-SMB/data.

Author contributions. AR conceived of the Stochastic Ice Sheet project. LU and AR designed the SMB study, with support from SC. LU wrote the code, made the figures, and drafted the manuscript. All authors contributed to editing the manuscript and approved its final form.

Competing interests. The authors have declared that no competing interests are present.

Acknowledgements. The authors thank GrSMBMIP participating teams led by Tijn Berends, Leo van Kampenhout, Uta Krebs-Kanzow, Ruth Mottram, Masashi Niwano, Glen Liston, and Brice Noël for their permission to use their model data, and Xavier Fettweis for facilitating access to GrSMBMIP and MAR output data.
The authors thank Matt Osman for ice core data consultation.
This research has been supported by the Heising-Simons Foundation (grant no. 2020-1965).

References

345   Andersen, K. K., Ditlevsen, P. D., Rasmussen, S. O., Clausen, H. B., Vinther, B. M., Johnsen, S. J., and Steffensen, J. P.: Retrieving a common accumulation record from Greenland ice cores for the past 1800 years, Journal of Geophysical Research: Atmospheres, 111, https://doi.org/https://doi.org/10.1029/2005JD006765, 2006.

Boers, N. and Rypdal, M.: Critical slowing down suggests that the western Greenland Ice Sheet is close to a tipping point, Proceedings of the National Academy of Sciences, 118, e2024192118, https://doi.org/https://doi.org/10.1073/pnas.2024192118, 2021.

350   Bos, M. S., Fernandes, R. M. S., Williams, S. D. P., and Bastos, L.: Fast error analysis of continuous GNSS observations with missing data, Journal of Geodesy, 87, 351–360, https://doi.org/10.1007/s00190-012-0605-0, 2013a.

Bos, M. S., Williams, S. D. P., Araújo, I. B., and Bastos, L.: The effect of temporal correlated noise on the sea level rate and acceleration uncertainty, Geophysical Journal International, 196, 1423–1430, https://doi.org/10.1093/gji/ggt481, 2013b.

Christian, J. E., Robel, A., Proistosescu, C., Roe, G., Koutnik, M., and Christianson, K.: The contrasting response of outlet glaciers to interior

355   and ocean forcing, 2020.

Edwards, T. L., Fettweis, X., Gagliardini, O., Gillet-Chaulet, F., Goelzer, H., Gregory, J. M., Hoffman, M., Huybrechts, P., Payne, A. J., Perego, M., Price, S., Quiquet, A., and Ritz, C.: Effect of uncertainty in surface mass balance–elevation feedback on projections of the future sea level contribution of the Greenland ice sheet, The Cryosphere, 8, 195–208, https://doi.org/10.5194/tc-8-195-2014, 2014.

Edwards, T. L., Nowicki, S., Marzeion, B., Hock, R., Goelzer, H., Seroussi, H., Jourdain, N. C., Slater, D. A., Turner, F. E., Smith, C. J.,

360   McKenna, C. M., Simon, E., Abe-Ouchi, A., Gregory, J. M., Larour, E., Lipscomb, W. H., Payne, A. J., Shepherd, A., Agosta, C., Alexander, P., Albrecht, T., Anderson, B., Asay-Davis, X., Aschwanden, A., Barthel, A., Bliss, A., Calov, R., Chambers, C., Champollion, N., Choi, Y., Cullather, R., Cuzzone, J., Dumas, C., Felikson, D., Fettweis, X., Fujita, K., Galton-Fenzi, B. K., Gladstone, R., Golledge, N. R., Greve, R., Hattermann, T., Hoffman, M. J., Humbert, A., Huss, M., Huybrechts, P., Immerzeel, W., Kleiner, T., Kraaijenbrink, P., Le clec'h, S., Lee, V., Leguy, G. R., Little, C. M., Lowry, D. P., Malles, J.-H., Martin, D. F., Maussion, F., Morlighem, M., O'Neill, J. F.,

365   Nias, I., Pattyn, F., Pelle, T., Price, S. F., Quiquet, A., Radić, V., Reese, R., Rounce, D. R., Rückamp, M., Sakai, A., Shafer, C., Schlegel, N.-J., Shannon, S., Smith, R. S., Straneo, F., Sun, S., Tarasov, L., Trusel, L. D., Van Breedam, J., van de Wal, R., van den Broeke, M., Winkelmann, R., Zekollari, H., Zhao, C., Zhang, T., and Zwinger, T.: Projected land ice contributions to twenty-first-century sea level rise, Nature, 593, 74–82, https://doi.org/10.1038/s41586-021-03302-y, 2021.

Fettweis, X., Hofer, S., Krebs-Kanzow, U., Amory, C., Aoki, T., Berends, C. J., Born, A., Box, J. E., Delhasse, A., Fujita, K., Gierz, P.,

370   Goelzer, H., Hanna, E., Hashimoto, A., Huybrechts, P., Kapsch, M.-L., King, M. D., Kittel, C., Lang, C., Langen, P. L., Lenaerts, J. T. M., Liston, G. E., Lohmann, G., Mernild, S. H., Mikolajewicz, U., Modali, K., Mottram, R. H., Niwano, M., Noël, B., Ryan, J. C., Smith, A., Streffing, J., Tedesco, M., van de Berg, W. J., van den Broeke, M., van de Wal, R. S. W., van Kampenhout, L., Wilton, D., Wouters, B., Ziemen, F., and Zolles, T.: GrSMBMIP: intercomparison of the modelled 1980–2012 surface mass balance over the Greenland Ice Sheet, The Cryosphere, 14, 3935–3958, https://doi.org/10.5194/tc-14-3935-2020, 2020.

375   Friedman, J., Hastie, T., and Tibshirani, R.: Sparse inverse covariance estimation with the graphical lasso, Biostatistics, 9, 432–441, https://doi.org/10.1093/biostatistics/kxm045, 2007.

Goelzer, H., Nowicki, S., Payne, A., Larour, E., Seroussi, H., Lipscomb, W. H., Gregory, J., Abe-Ouchi, A., Shepherd, A., Simon, E., Agosta, C., Alexander, P., Aschwanden, A., Barthel, A., Calov, R., Chambers, C., Choi, Y., Cuzzone, J., Dumas, C., Edwards, T., Felikson, D., Fettweis, X., Golledge, N. R., Greve, R., Humbert, A., Huybrechts, P., Le clec'h, S., Lee, V., Leguy, G., Little, C., Lowry, D. P., Morlighem,

380   M., Nias, I., Quiquet, A., Rückamp, M., Schlegel, N.-J., Slater, D. A., Smith, R. S., Straneo, F., Tarasov, L., van de Wal, R., and van den

Broeke, M.: The future sea-level contribution of the Greenland ice sheet: a multi-model ensemble study of ISMIP6, The Cryosphere, 14, 3071–3096, https://doi.org/10.5194/tc-14-3071-2020, 2020.

Hanna, E., Huybrechts, P., Cappelen, J., Steffen, K., Bales, R. C., Burgess, E., McConnell, J. R., Peder Steffensen, J., Van den Broeke, M., Wake, L., Bigg, G., Griffiths, M., and Savas, D.: Greenland Ice Sheet surface mass balance 1870 to 2010 based on Twentieth Century Reanalysis, and links with global climate forcing, Journal of Geophysical Research: Atmospheres, 116, https://doi.org/https://doi.org/10.1029/2011JD016387, 2011.

Hanna, E., Navarro, F. J., Pattyn, F., Domingues, C. M., Fettweis, X., Ivins, E. R., Nicholls, R. J., Ritz, C., Smith, B., Tulaczyk, S., Whitehouse, P. L., and Zwally, H. J.: Ice-sheet mass balance and climate change, Nature, 498, 51–59, https://doi.org/10.1038/nature12238, 2013.

Hinkel, J., Church, J. A., Gregory, J. M., Lambert, E., Le Cozannet, G., Lowe, J., McInnes, K. L., Nicholls, R. J., van der Pol, T. D., and van de Wal, R.: Meeting User Needs for Sea Level Rise Information: A Decision Analysis Perspective, Earth's Future, 7, 320–337, https://doi.org/https://doi.org/10.1029/2018EF001071, 2019.

Hu, W. and Castruccio, S.: Approximating the Internal Variability of Bias-Corrected Global Temperature Projections with Spatial Stochastic Generators, Journal of Climate, 34, 8409 – 8418, https://doi.org/10.1175/JCLI-D-21-0083.1, 2021.

Jevrejeva, S., Frederikse, T., Kopp, R. E., Le Cozannet, G., Jackson, L. P., and van de Wal, R. S. W.: Probabilistic Sea Level Projections at the Coast by 2100, Surveys in Geophysics, 40, 1673–1696, https://doi.org/10.1007/s10712-019-09550-y, 2019.

King, M. A. and Watson, C. S.: Antarctic Surface Mass Balance: Natural Variability, Noise, and Detecting New Trends, Geophysical Research Letters, 47, e2020GL087 493, https://doi.org/https://doi.org/10.1029/2020GL087493, 2020.

Kopp, R. E., Horton, R. M., Little, C. M., Mitrovica, J. X., Oppenheimer, M., Rasmussen, D. J., Strauss, B. H., and Tebaldi, C.: Probabilistic 21st and 22nd century sea-level projections at a global network of tide-gauge sites, Earth's Future, 2, 383–406, https://doi.org/https://doi.org/10.1002/2014EF000239, 2014.

Krebs-Kanzow, U., Gierz, P., Rodehacke, C. B., Xu, S., Yang, H., and Lohmann, G.: The diurnal Energy Balance Model (dEBM): a convenient surface mass balance solution for ice sheets in Earth system modeling, The Cryosphere, 15, 2295–2313, https://doi.org/10.5194/tc-15-2295-2021, 2021.

Kuttruf, S.: Python code for fractional differencing of pandas time series, https://gist.github.com/skuttruf/fb82807ab0400fba51c344313eb43466 [Source code], 2019.

Le Cozannet, G., Nicholls, R. J., Hinkel, J., Sweet, W. V., McInnes, K. L., Van de Wal, R. S. W., Slangen, A. B. A., Lowe, J. A., and White, K. D.: Sea Level Change and Coastal Climate Services: The Way Forward, Journal of Marine Science and Engineering, 5, https://doi.org/10.3390/jmse5040049, 2017.

Lenaerts, J. T. M., Medley, B., van den Broeke, M. R., and Wouters, B.: Observing and Modeling Ice Sheet Surface Mass Balance, Reviews of Geophysics, 57, 376–420, https://doi.org/https://doi.org/10.1029/2018RG000622, 2019.

Luo, X. and Lin, T.: A Semi-Empirical Framework for ice sheet response analysis under Oceanic forcing in Antarctica and Greenland, Climate Dynamics, https://doi.org/10.1007/s00382-022-06317-x, 2022.

Mohammadi, H., Challenor, P., and Goodfellow, M.: Emulating dynamic non-linear simulators using Gaussian processes, Computational Statistics & Data Analysis, 139, 178–196, https://doi.org/https://doi.org/10.1016/j.csda.2019.05.006, 2019.

Mouginot, J. and Rignot, E.: Glacier catchments/basins for the Greenland Ice Sheet, Dryad Dataset, https://doi.org/10.7280/D1WT11, https://doi.org/10.7280/D1WT11, 2019.

Pedregosa, F., Varoquaux, G., Gramfort, A., Michel, V., Thirion, B., Grisel, O., Blondel, M., Prettenhofer, P., Weiss, R., Dubourg, V., Vanderplas, J., Passos, A., Cournapeau, D., Brucher, M., Perrot, M., and Duchesnay, E.: Scikit-learn: Machine Learning in Python, Journal

420   of Machine Learning Research, 12, 2825–2830, 2011.

Rahmstorf, S.: A Semi-Empirical Approach to Projecting Future Sea-Level Rise, Science, 315, 368–370, https://doi.org/10.1126/science.1135456, 2007.

Sacks, J., Welch, W. J., Mitchell, T. J., and Wynn, H. P.: Design and Analysis of Computer Experiments, Statistical Science, 4, 409–423, https://doi.org/10.1214/ss/1177012413, 1989.

425   Seabold, S. and Perktold, J.: statsmodels: Econometric and statistical modeling with python, in: 9th Python in Science Conference, https://doi.org/10.25080/Majora-92bf1922-011, 2010.

Sellevold, R., van Kampenhout, L., Lenaerts, J. T. M., Noël, B., Lipscomb, W. H., and Vizcaino, M.: Surface mass balance downscaling through elevation classes in an Earth system model: application to the Greenland ice sheet, The Cryosphere, 13, 3193–3208, https://doi.org/10.5194/tc-13-3193-2019, 2019.

430   Seroussi, H., Nowicki, S., Payne, A. J., Goelzer, H., Lipscomb, W. H., Abe-Ouchi, A., Agosta, C., Albrecht, T., Asay-Davis, X., Barthel, A., Calov, R., Cullather, R., Dumas, C., Galton-Fenzi, B. K., Gladstone, R., Golledge, N. R., Gregory, J. M., Greve, R., Hattermann, T., Hoffman, M. J., Humbert, A., Huybrechts, P., Jourdain, N. C., Kleiner, T., Larour, E., Leguy, G. R., Lowry, D. P., Little, C. M., Morlighem, M., Pattyn, F., Pelle, T., Price, S. F., Quiquet, A., Reese, R., Schlegel, N.-J., Shepherd, A., Simon, E., Smith, R. S., Straneo, F., Sun, S., Trusel, L. D., Van Breedam, J., van de Wal, R. S. W., Winkelmann, R., Zhao, C., Zhang, T., and Zwinger, T.: ISMIP6 Antarctica: a multi-

435   model ensemble of the Antarctic ice sheet evolution over the 21st century, The Cryosphere, 14, 3033–3070, https://doi.org/10.5194/tc-14-3033-2020, 2020.

Sriver, R. L., Lempert, R. J., Wikman-Svahn, P., and Keller, K.: Characterizing uncertain sea-level rise projections to support investment decisions, PLOS ONE, 13, 1–35, https://doi.org/10.1371/journal.pone.0190641, 2018.

Titus, J. G. and Narayanan, V.: The risk of sea level rise, Climatic Change, 33, 151–212, https://doi.org/10.1007/BF00140246, 1996.

440   Verjans, V., Robel, A. A., Seroussi, H., Ultee, L., and Thompson, A. F.: The Stochastic Ice-Sheet and Sea-Level System Model v1.0 (StISSM v1.0), Geoscientific Model Development, 15, 8269–8293, https://doi.org/10.5194/gmd-15-8269-2022, 2022.

Walsh, K. J. E., Betts, H., Church, J., Pittock, A. B., McInnes, K. L., Jackett, D. R., and McDougall, T. J.: Using Sea Level Rise Projections for Urban Planning in Australia, Journal of Coastal Research, 20, 586–598, https://doi.org/10.2112/1551-5036(2004)020[0586:USLRPF]2.0.CO;2, 2004.

445   Williams, S. D. P., Moore, P., King, M. A., and Whitehouse, P. L.: Revisiting GRACE Antarctic ice mass trends and accelerations considering autocorrelation, Earth and Planetary Science Letters, 385, 12–21, https://doi.org/https://doi.org/10.1016/j.epsl.2013.10.016, 2014.

Wilton, D. J., Jowett, A., Hanna, E., Bigg, G. R., Van Den Broeke, M. R., Fettweis, X., and Huybrechts, P.: High resolution (1 km) positive degree-day modelling of Greenland ice sheet surface mass balance, 1870–2012 using reanalysis data, Journal of Glaciology, 63, 176–193, https://doi.org/DOI: 10.1017/jog.2016.133, 2017.

450   Wouters, B., Bamber, J. L., van den Broeke, M. R., Lenaerts, J. T. M., and Sasgen, I.: Limits in detecting acceleration of ice sheet mass loss due to climate variability, Nature Geoscience, 6, 613–616, https://doi.org/10.1038/ngeo1874, 2013.